Configuration of PKCα-C2 Domain Bound to Mixed SOPC/SOPS Lipid Monolayers

Chiu-Hao Chen,[†] Šárka Málková,[†] Sai Venkatesh Pingali,[†] Fei Long,[‡] Shekhar Garde,[§] Wonhwa Cho,[‡] and Mark L. Schlossman[†*]

[†]Department of Physics and [‡]Department of Chemistry, University of Illinois at Chicago, Chicago, Illinois; and [§]Department of Chemical and Biological Engineering and Center for Biotechnology and Interdisciplinary Studies, Rensselaer Polytechnic Institute, Troy, New York

ABSTRACT X-ray reflectivity measurements are used to determine the configuration of the C2 domain of protein kinase Cα (PKCα-C2) bound to a lipid monolayer of a 7:3 mixture of 1-stearoyl-2-oleoyl-*sn*-glycero-3-phosphocholine and 1-stearoyl-2-oleoyl-*sn*-glycero-3-phosphoserine supported on a buffered aqueous solution. The reflectivity is analyzed in terms of the known crystallographic structure of PKCα-C2 and a slab model representation of the lipid layer. The configuration of lipid-bound PKCα-C2 is described by two angles that define its orientation, $\theta = 35^\circ \pm 10^\circ$ and $\varphi = 210^\circ \pm 30^\circ$, and a penetration depth ($=7.5 \pm 2$ Å) into the lipid layer. In this structure, the β-sheets of PKCα-C2 are nearly perpendicular to the lipid layer and the domain penetrates into the headgroup region of the lipid layer, but not into the tailgroup region. This configuration of PKCα-C2 determined by our x-ray reflectivity is consistent with many previous findings, particularly mutational studies, and also provides what we believe is new molecular insight into the mechanism of PKCα enzyme activation. Our analysis method, which allows us to test all possible protein orientations, shows that our data cannot be explained by a protein that is orientated parallel to the membrane, as suggested by earlier work.

INTRODUCTION

Peripheral membrane proteins that are important for cell signaling and vesicle trafficking are specifically targeted to different cell membranes in response to various stimuli, including calcium and lipid mediators (1). Because the function and regulation of these proteins depends on their interaction with the membrane (2,3), recent work has focused on determining their membrane-bound orientation and depth of membrane penetration (4–7). These structural parameters have been determined by mutational studies, fluorescence measurements, electron spin resonance (EPR) measurements, and x-ray reflectivity measurements of peripheral membrane proteins bound to model membranes, such as lipid bilayer vesicles or lipid monolayers (4,8–10). In particular, we have shown recently that x-ray reflectivity can provide a direct, detailed, and quantitative determination of the membrane bound configuration of lipid binding domains, including C2 and PX domains (9,11). We show that an improved method of analysis of the x-ray reflectivity allows us to efficiently analyze the entire space of all protein orientations. This yields a more complete and accurate determination of the bound configuration. Application of this technique to the C2 domain of protein kinase Cα (PKCα-C2) bound to mixed lipid monolayers resolves a controversy about the bound configuration of this domain.

PKCα is a member of the classical PKC family that is important in cell signaling (12–14). The C2 domain of PKCα is an independent membrane-targeting module that is composed of an eight-stranded β sandwich with flexible loops on either end (Fig. 1 *A*). Three Ca^{2+} binding loops (CBL1, CBL2, CBL3), located at one end of the domain structure, bind two or three calcium ions in a highly cooperative manner due to the presence of five highly conserved Asp residues (5,6,15). The coordination of calcium ions alters the electrostatic potential of the C2 domain (16), which accelerates its association to the plasma membrane where it recognizes phosphatidylserine (PS) (6,17,18) and phosphatidylinositol-4,5-bisphosphate (PIP_2) (19–21). Wonhwa Cho reported recently that the interaction of the Ca^{2+} binding loops of PKCα-C2 with Ca^{2+} and PS drives its membrane binding whereas the interaction of its cationic β-groove residues with PIP_2 augments the membrane binding (22). These findings indicate that the direct interaction of PKCα-C2 with PS is a critical step in the mechanism of cellular plasma membrane translocation of PKCα.

The CBLs of PKCα-C2 domain have been recognized as a critical docking region that interacts with anionic PS molecules in the membrane (16,23,24). It has been suggested that PKCα-C2 domain can bind to PS-containing lipid bilayers by two distinct orientations, i.e., perpendicular and parallel to the membrane surface (25). Both are consistent with the critical role of the PKCα-C2 CBLs as a PS docking region. In the perpendicular model (Fig. 1 *A*), the docking surface is localized to the CBLs and the β-strands lie nearly perpendicular to the membrane surface. In contrast, in the parallel model (Fig. 1 *B*), the β-strands are oriented approximately parallel to the membrane surface, which allows Lys^{205}, as well as Ca^{2+} ions, to interact with PS headgroups (6).

A crystallographic study of PKCα-C2 complexed with a short-chain PS, 1,2-dicaproyl-*sn*-phosphatidylserine (DCPS) and Ca^{2+} ions led to the suggestion that PKCα-C2 would orient in the parallel model when bound to a membrane (6). Two recent EPR measurements of site-specific

Submitted April 14, 2009, and accepted for publication August 24, 2009.

*Correspondence: schloss@uic.edu

Editor: Huey W. Huang.

0006-3495/09/11/2794/9 $2.00

doi: 10.1016/j.bpj.2009.08.037

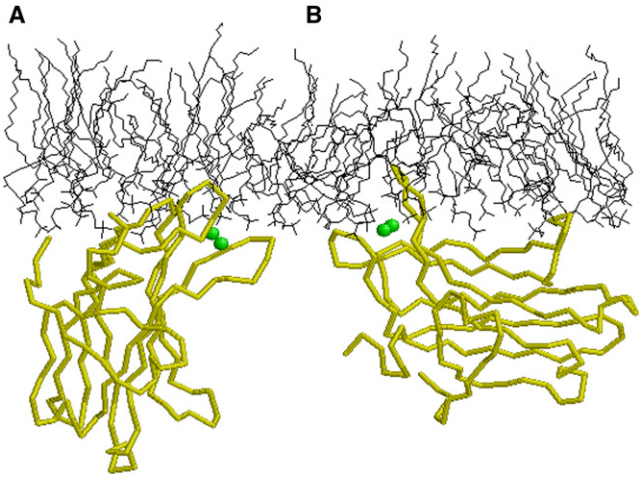

FIGURE 1 PKCα−C2 domain with Ca^{2+} (*spheres* (*green*)) bound to a lipid layer (52) (*color online*). (*A*) In a perpendicular model, the β-strands orient essentially perpendicular to the membrane surface and the Ca^{2+} binding pocket provides the primary interaction between the domain and the lipids. (*B*) In a parallel model, the β-strands are essentially parallel to the membrane surface. This allows interactions between lipids and other residues, such as those in β3-β4-sheets, in addition to interactions with the Ca^{2+} binding pocket.

spin-labeled PKCα-C2 have also suggested that PKCα-C2 is oriented parallel to the membrane (25,26). However, the parallel model is not consistent with many mutational studies (15,17,27), as described in further detail in the Discussion section. Collectively, the existing studies do not determine unambiguously the membrane bound orientation of the PKCα-C2 domain. Because the reported discrepancy between EPR and mutational studies may derive from the introduction of bulky unnatural spin labels that may disturb the system, we carried out a detailed structural analysis of membrane bound orientation of unlabeled PKCα-C2 by our x-ray reflectivity analysis.

To determine the membrane-bound configuration of PKCα-C2, we carried out x-ray reflectivity measurements (9,28,29) from a mixed lipid monolayer (7:3 SOPC/SOPS, see Materials) supported on the surface of a buffered aqueous solution that contains PKCα-C2 domain. X-ray reflectivity determines the variation of electron density with depth through the surface that, in this case, consists of a layer of lipids along with bound PKCα-C2 domains. This electron density is then interpreted in terms of the arrangement of PS lipids and PKCα-C2 domains. Significant conformational rearrangement of the internal structure of the C2 domain on binding to phospholipids is not expected (6,7,10,30). Therefore, we incorporated the known structure of PKCα-C2 from the Protein Data Bank (PDB) (ID 1dsy) (6) into our analysis of the x-ray reflectivity. Our results show that the reflectivity data are consistent with two slightly different bound configurations, both falling within the confines of the perpendicular model. Parallel orientations of PKCα-C2 (6,25,26) are not consistent with our x-ray reflectivity measurements. The preferred configuration has an orientation given by $\theta = 35^\circ \pm 10^\circ$ and $\varphi = 210^\circ \pm 30^\circ$ and penetrates a distance of 7.5 $\pm$ 2 Å into the lipid headgroup. The PKCα-C2 domain does not insert into the hydrophobic region of the lipid layer. The calcium binding loops CBL1 and CBL2 penetrate into the lipid headgroup whereas CBL3 is located adjacent to the headgroup. Furthermore, this configuration allows us to postulate a mechanism for the activation of protein kinase Cα.

MATERIALS AND METHODS

Materials

KCl, $CaCl_2$, and HEPES (*N*-(2-hydroxyethl)piperazine-*N*′-2-ethanesulfonic acid) from Fisher Scientific (Hampton, NH) and EGTA (ethyleneglycol-*O*, *O*′-bis(2-aminoethyl)-*N*, *N*, *N*′, *N*′-tetraacetic acid) from Sigma (St. Louis, MO) were used as obtained. Stock solutions of 1-stearoyl-2-oleoyl-*sn*-glycero-3-phosphocholine (SOPC) and 1-stearoyl-2-oleoyl-*sn*-glycero-3-phosphoserine (SOPS) (7:3 molar ratio) in chloroform and 1-palmitoyl-2-{6-[(7-*nitro*-2-1,3-benzoxadiazol-4-yl)amino]-hexanoyl}-*sn*-glycero-3-phosphocholine (NBD PC) in chloroform were purchased from Avanti Polar Lipids and used without further purification. Spreading solutions were prepared by diluting the stock solution with freshly opened bottles of chloroform (Sigma). Expression and purification of the C2 domain of PKCα were carried out as described previously (15). The domain sequence of the purified protein is composed of M^{152}DHH^{155} (additional residues from purification protocol), T^{156} to N^{287} (from 1DSY PDB file (6)), and L^{288}EHHHHHH^{295} (additional residues from purification protocol). The method for modeling the additional residues was described in the previous work (9). A PDB file of the composition of additional residues and 1DSY is provided in the Supporting Material.

Sample preparation and surface pressure measurements

To prepare a sample for study by x-ray reflectivity ~10 μL of 1 mM SOPC and SOPS (7:3) in chloroform was added dropwise onto the surface of a pH 7.0 aqueous solution containing aqueous 20 mM HEPES buffer, 0.1 M KCl, and 0.1 mM $CaCl_2$ in a circular Teflon trough of 72 mm diameter and ~40 mL total volume. The ratio of 7:3 SOPC/SOPS was chosen to be consistent with earlier biochemical measurements on similar systems (31).The resulting lipid monolayer was equilibrated for 2 h and the reflectivity was measured. An amount of PKCα-C2 slightly greater than the amount required to saturate the lipid layer (i.e., >240 μg; see the Supporting Material) was then injected into the subphase, the system equilibrated for 1 h with continuous slow stirring, the stir bar stopped, the system allowed to briefly relax, and the reflectivity was measured. The surface pressure was monitored throughout the experiment, including equilibration and x-ray measurement, with a filter paper Wilhelmy plate and a Nima surface pressure sensor PS-4. Typical variations in surface pressure were $\pm$0.5 mN/m and appeared as random fluctuations during the period (i.e., 6–8 h) of the measurement of the lipid layer with and without bound PKCα-C2. We report on data from three separate experiments on monolayers with similar initial surface pressures (24.6, 26.7, and 24.9 mN/m) and similar changes in pressure on adding PKCα-C2 ($\Delta\pi = 2.0 \pm 0.5$, 2.6 $\pm$ 0.5, and 3.1 $\pm$ 0.5 mN/m, respectively). Note that fluorescence microscopy was used to verify the absence of micrometer-scale or larger domains (see the Supporting Material).

X-ray reflectivity measurements

X-ray reflectivity experiments were carried out at beamline X19C at the National Synchrotron Light Source (Brookhaven National Laboratory, Upton, NY) with a liquid surface reflectometer described in detail elsewhere

(32). Reflectivity is measured as a function of the wave vector transfer Q_z by varying the incident angle α and measuring the intensity of x-rays reflected at the angle α. The wave vector transfer of the reflected x-rays, $\boldsymbol{Q}$, is solely in the z-direction normal to the buffer surface with $Q_z = (4\pi/\lambda)\ \sin\alpha$, where $\lambda = 1.54 \pm 0.003$ Å is the x-ray wavelength. Reflectivity probes variations in electron density as a function of depth into the surface.

The reflectivity $R(Q_z)$ represents the reflected x-ray intensity divided by the x-ray intensity measured before the sample. In addition, background scattering is measured and subtracted as described elsewhere (32). To make the features of the reflectivity curve more evident, $R(Q_z)$ is divided by $R_F(Q_z)$, the Fresnel reflectivity calculated for an ideal, smooth, and flat interface (33). Deviations of the measured reflectivity, $R(Q_z)$, from the Fresnel reflectivity, $R_F(Q_z)$, show the presence of interfacial structure as a function of surface depth. In this case, the structure is due to the lipid monolayer supported on the buffer surface and the PKCα-C2 domains bound to the lipid monolayer. No radiation damage was detected during the measurements, as indicated by the surface pressure stability and the reproducibility of the x-ray reflectivity data after repeated measurements on the same sample (data not shown) (9).

Data analysis

We outline our analysis methodology (see the Supporting Material for details). X-ray reflectivity measurements as a function of the reflection angle are usually analyzed by 1), assuming a model (a functional form) for the electron density as a function of depth z into the surface, but averaged over the in-plane x-y direction (the so-called electron density profile); 2), computing the reflectivity from this model; and 3), comparing the computed reflectivity to the measured reflectivity by the use of a nonlinear least-squares fitting procedure that adjusts parameters in the model to yield a best fit to the data (33–35).

We model the electron density profile of the lipid monolayer as consisting of two slabs of uniform electron density that correspond to the lipid tailgroups and headgroups (33). In studies of a monolayer plus protein system (Fig. 2), other authors have described the protein as an additional slab of uniform electron density (8,29,36–40). However, a protein like PKCα-C2 has a robust structure with a well-defined arrangement of atoms and, therefore, a specific electron density profile for a given orientation. Describing this protein electron density profile as a single slab of uniform electron density results in a loss of information when reflectivity is analyzed. Previously, we introduced the use of the protein structure, taken from crystallography or NMR studies of protein domains, into the analysis of x-ray reflectivity from cPLA$_2\alpha$-C2 and p40^{phox}-PX domains adsorbed onto Langmuir monolayers of lipids (9,11). The use of a crystal structure has been applied recently to a neutron reflectivity study of hemolysin channels, although the orientation was fixed (41).

The purpose of our analysis is to determine the orientation of the protein with respect to the plane of the lipid layer, the penetration depth of the protein into the lipid layer, the fraction of interface covered by the protein, as well as to characterize the thickness and electron density of the lipid tailgroup and headgroup (L_{tail}, ρ_{tail}, L_{head}, and ρ_{head}, respectively). Fig. 2 illustrates a PKCα-C2 domain at a particular orientation that has penetrated partially into the headgroup region of the lipid monolayer, but not into the tailgroup region. It also illustrates N layers, each of uniform electron density in the x-y plane that is used to describe the electron density profile of the interface. The first layer is used to model the electron density of the tailgroup with two fitting parameters—its average electron density ρ_{tail} and thickness L_{tail}. The tailgroup is located between the interfacial positions $z = 0$ and $z = -L_{tail}$. The second layer models the top part of the headgroup that is not penetrated by the protein. Subsequent layers that extend down to the position of the headgroup/buffer interface (at $z = -L_{tail} - L_{head}$) model a region of the interface occupied by both the top part of the protein and lipid headgroups. The remaining layers model a region occupied partially by the bottom part of the protein and partially by the aqueous buffer, although we do not exclude the possibility that the protein can fully cover the interface. Our model also allows for the possibility that the protein domain penetrates into the tailgroup region or does not penetrate the lipid monolayer at all, although we have discussed only the case illustrated in Fig. 2 because it is most relevant to the analysis of our data on PKCα-C2.

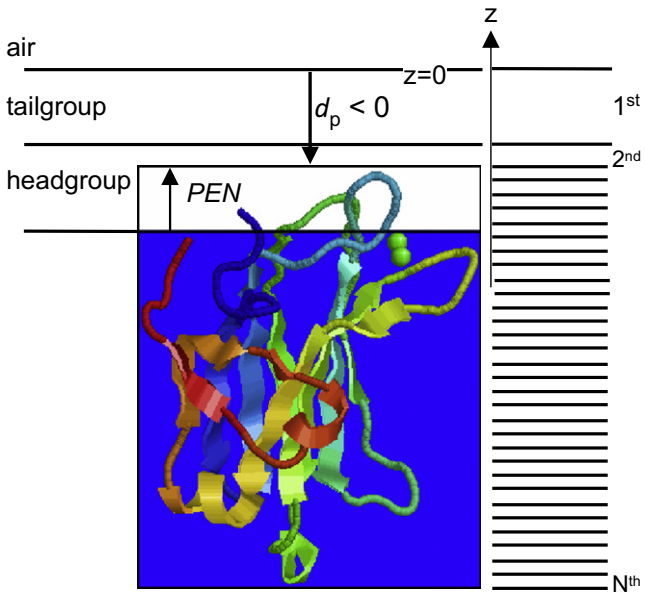

FIGURE 2 Illustration of the model for protein-membrane binding (*color online*). The intrinsic electron density profile $\rho_i(z)$ consists of $N + 2$ layers with $N + 1$ interfaces. Two of these layers are the bulk air and buffer; the remaining N layers describe the lipids and proteins. The positive z axis is above the lipid layer; depths within the lipid layer, protein, or buffer are indicated by negative values of z. Protein penetration into the lipid layer PEN is positive in this drawing. See Supporting Material for a description of parameter d_p.

The protein is characterized by using coordinates from the PDB file (6) of the PKCα-C2 domain (1DSY) plus additional residues from the purification protocol (see Materials and Methods). The software Molprobity was used to restore the hydrogen atoms onto the protein (42). We chose three atoms in the protein to define a protein coordinate system, then rotated the protein with respect to a coordinate system defined by the lipid layer (equivalently, the buffer/air surface). To account for the fact that part of the protein is located in the buffer and part in the lipid layer, a confining mathematical box is drawn around the protein. In practice, two boxes are used. In one the empty space in the box is filled with aqueous buffer by assigning to that volume the electron density of the buffer, in the other it is left empty. Part of the box with buffer is used to describe the corresponding part of the protein that is in the buffer below the lipid layer. The remainder of the protein that inserts into the lipid layer is described by the corresponding part of the box whose empty space was left empty; our analysis method fills this empty space by electron density from the lipid layer (e.g., the headgroup in the case illustrated in Fig. 2).

For a given orientation, the electron density profile of the box with protein is calculated by slicing the box into thin layers along the surface normal (Fig. 2), then counting the number of electrons in each layer and dividing by the layer volume. These profiles are produced for a complete range of protein orientations. The protein profile for a given orientation is combined with a two-slab model of the lipid monolayer in a nonlinear least squares fitting to the x-ray reflectivity data in which six parameters are fit (L_{tail}, ρ_{tail}, L_{head}, and ρ_{head}, the distance penetration (PEN) that the protein penetrates into the lipid layer (Fig. 2), and the coverage COV, i.e., the fraction of surface covered by the protein-filled boxes). This procedure yields a goodness of fit parameter χ^2 for each protein orientation. Comparison of these χ^2 values determines the best-fit orientation and the accompanying best-fit values for the six fitting parameters.

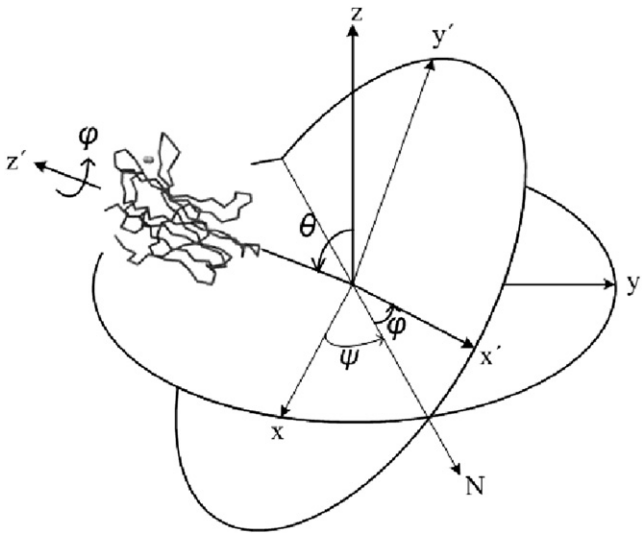

FIGURE 3 Euler angles used to describe the orientation of PKCα-C2 domain (attached to x'-y'-z' coordinate system) with respect to the lipid monolayer in the x-y-z coordinate system (positive z axis points upward, away from the aqueous buffer). The orientation of the PKCα-C2 domain is characterized by two Euler angles, θ and φ. The angle θ is a polar rotation of the protein z' axis from the surface normal and the angle φ is an azimuthal rotation about the protein z' axis. The angle ψ, between the x axis and the line of nodes N, represents an azimuthal rotation of the domain about the z axis and within the plane of the monolayer. This rotation does not change the electron density profile averaged over the surface x-y plane, therefore x-ray reflectivity is insensitive to variations in ψ.

X-ray reflectivity data were fit to the entire range of orientational angles of the PKCα-C2 domain. The angle θ measures the angle between the protein's z' axis and the surface normal z axis, whereas the angle φ is an azimuthal rotation about the direction of the z' axis (Fig. 3). Initially, fitting was carried out for values of θ spaced by 10° over the range from 0 to π and for values of φ spaced by 30° over the range from 0 to 2π. This procedure determined the approximate location of the best-fit orientations. Then, a finer 1° spacing of θ and φ values was used to locate the best-fit orientations precisely. Contour plots of the goodness of fit parameter χ^2 as a function of θ and φ, similar to that shown in Fig. 4 (discussed below), were produced for the three data sets.

RESULTS

Analysis of the x-ray reflectivity data was carried out for measurements from three separate samples, which differed slightly in the initial value of the surface pressure of the monolayer and in the change in surface pressure on adsorption of the protein domain (see Materials and Methods). Fig. 4 shows the χ^2 contour plot that results from averaging the χ^2 contour plots from analyses of the three separate measurements. Two best-fit orientations were obtained whose χ^2 values were within one statistical standard deviation (SD) of each other. These orientations are given by $\theta = 35° \pm 10°$, $\varphi = 210° \pm 30°$ and $\theta = 35° +3°/-8°$, $\varphi = 0° +10°/-5°$. The fitting parameters for each of these two orientations are listed in Table 1, where the uncertainties were computed by the appropriate mapping of χ^2-space (43). Fits to the reflectivity data for the two best-fit orientations for

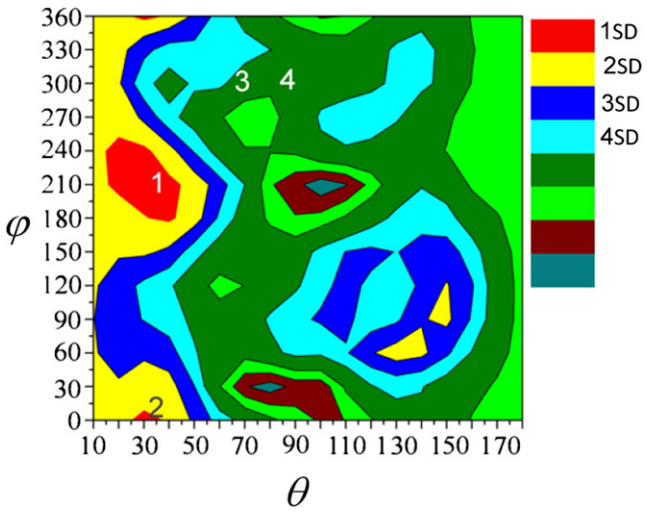

FIGURE 4 Contour plot of the goodness of fit parameter χ^2 (by *grayscale* or *color*) of fits to the x-ray reflectivity data for the PKCα-C2 domain oriented at angles θ and φ (*color online*). This plot was produced by averaging the χ^2 contour plots from measurements of three samples. The best fits were excellent (see Fig. 5) with a $\chi^2 = 5.9$ as determined by our use of counting statistics to calculate error bars on individual data points. The two best-fit orientations are indicated by the position of the numbers "1" ($\theta = 35°$ and $\varphi = 210°$) and "2" ($\theta = 35°$ and $\varphi = 0°$). The position of the numbers "3" ($\theta = 68°$ and $\varphi = 300°$) and "4" ($\theta = 90°$ and $\varphi = 300°$) indicate models proposed in Malmberg and Falke (26) and Verdaguer et al. (6), respectively. The four lowest bands of χ^2 (see legend) correspond to deviations of one to four standard deviations (SD) from the best fits. For example, the literature conformation whose angles are indicated by position 3 ($\theta = 68°$ and $\varphi = 300°$), is more than four SD away from the best fit. This means that if the angles $\theta = 68°$ and $\varphi = 300°$ are fixed, but the other free parameters are fit to the data, the resultant fit is more than four SD away from the best fit (43).

one of the samples are shown in Fig. 5, which shows that they are nearly identical. This is a consequence of the fact that the electron density profiles for the two best-fit orientations, one of which is shown in the inset to Fig. 5, are essentially identical.

Representations of the two best-fit monolayer-bound structures of the PKCα-C2 domain are shown in Fig. 6. In

TABLE 1 Parameters that describe the adsorption of PKCα-C2 domain to a mixed lipid layer of SOPC and SOPS for the two best-fit orientations determined from x-ray reflectivity measurements

	$\theta = 35° \pm 10°$ $\varphi = 210° \pm 30°$	$\theta = 35°(+3°/-8°)$ $\varphi = 0°(+10°/-5°)$
Penetration (PEN) (Å)	7.5 ± 2	5.8 ± 1.5
Coverage (COV)	0.44 ± 0.04	0.46 ± 0.04
L_{tail} (Å)	10.7 ± 0.1	10.8 ± 0.1
L_{head} (Å)	10.4 ± 0.4	10.9 ± 0.4
ρ_{tail} (electrons/Å^3)	0.21 ± 0.01	0.23 ± 0.01
ρ_{head} (electrons/Å^3)	0.44 ± 0.01	0.45 ± 0.01
Roughness (σ) (Å)	3.38	3.38
A_{box} (Å^2)	1663	1815
A_p area per protein (Å^2)	3800 ± 350	4000 ± 350

Parameters PEN, COV, L_{tail}, L_{head}, ρ_{tail}, and ρ_{head} are fitting parameters.

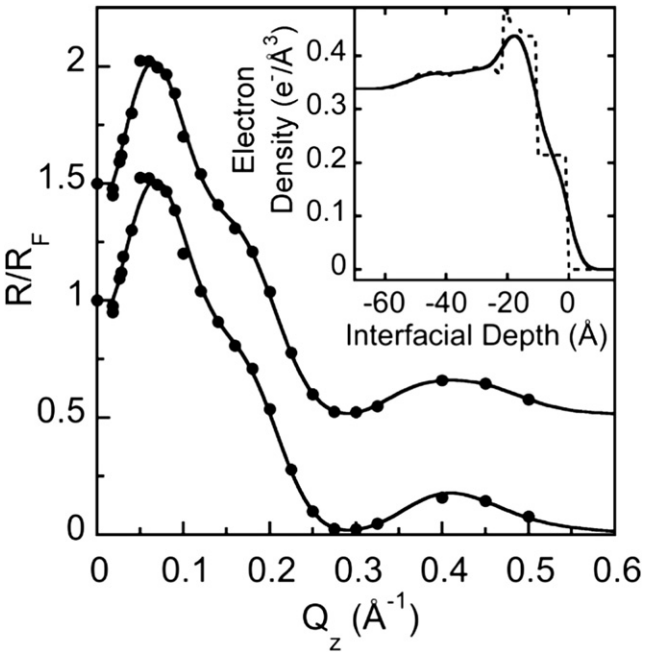

FIGURE 5 X-ray reflectivity normalized to the Fresnel reflectivity from one sample. Lines represent fits to the two best-fit orientations, ($\theta = 35°$, $\varphi = 210°$) and ($\theta = 35°$, $\varphi = 0°$), where the latter was displaced by +0.5 for clarity. Inset shows the electron density profile as a function of interfacial depth for the $\theta = 35°$, $\varphi = 210°$ orientation. The dashed line represents the intrinsic electron density profile (with zero interfacial roughness) for this orientation to illustrate the underlying features of the model.

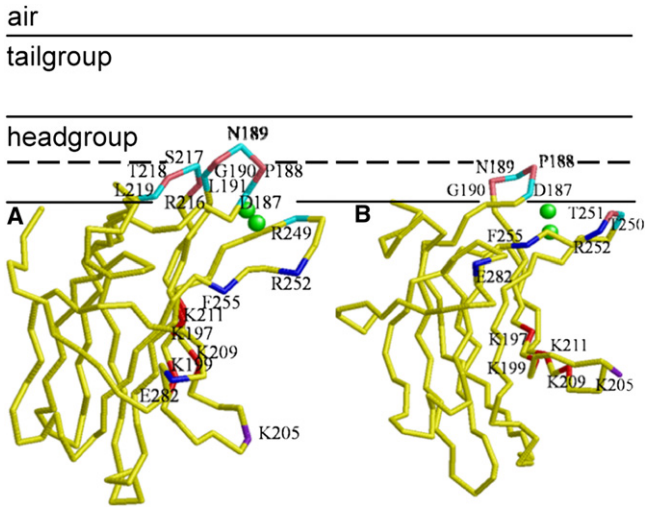

FIGURE 6 Backbone representations of the two best-fit configurations (*color online*). The dashed line indicates the average level of the lipid phosphates that lies close to the mid-plane of the lipid headgroup. (*A*) $\theta = 35°$, $\varphi = 210°$ orientation with a protein penetration of 7.5 ± 2 Å, and (*B*) $\theta = 35°$, $\varphi = 0°$ orientation with a protein penetration of 5.8 ± 1.5 Å. Calcium binding loops CBL1 consists of residues 187–193, CBL2 consists of 216–219, and CBL3 consists of 245–254 (15). In configuration *A* CBL1 and CBL2 penetrate the lipid layer, but in configuration *B* only CBL1 penetrates the layer. Residues R252, F255, and E282 are involved in interdomain interactions with C1A domain (47) and labeled in blue. The residues K197, K199, K209, and K211, in *red*, are a lysine-rich cluster (48). Residue K205 is in purple. The spheres (*green online*) indicate the Ca^{2+} ions.

the $\theta = 35°$, $\varphi = 0°$ orientation (Fig. 6 *B*), the residues Asp^{187}, Pro^{188}, Asn^{189} and Gly^{190} in CBL1 penetrate into the lipid headgroup. The residue Pro^{188} penetrates most deeply into the lipid monolayer. The location of polar and charged residues of the PKCα-C2 domain with respect to polar or charged regions of the lipids can be judged approximately by assuming an average orientation of the lipids in the monolayer. This orientation is given by x-ray and neutron diffraction studies of multilamellar DOPC bilayers (44,45) and is assumed to be similar to the average orientation of the SOPC and SOPS lipids that are used in this study. This orientation places the lipid phosphate groups ~5 Å (44–46) above the lipid/buffer interface, as indicated by the dashed line in Fig. 6. Under the assumption that the region of the protein that penetrates the lipid layer does not change its conformation from that given by crystallography, Fig. 6 *B* shows, for example, that the polar residue Asn^{189} is close to the phosphate plane. Similarly the residues Thr^{250} and Thr^{251} are close to the lipid/buffer interface. The Ca^{2+} ion Ca2 also is very close to the lipid-buffer interface, placing it near the negatively charged COO^- of the lipid. The Ca^{2+} ion Ca1 is further away by several angstroms. The approximate relative locations that we have identified allow for hydrogen bonding and favorable electrostatic interactions between the C2 domain and the SOPS headgroups.

In the $\theta = 35°$, $\varphi = 210°$ orientation (Fig. 6 *A*), the residues that penetrate into the lipid headgroup region are Asp^{187}, Pro^{188}, Asn^{189}, Gly^{190}, and Leu^{191} in CBL1 and Arg^{216}, Ser^{217}, Thr^{218}, and Leu^{219} in CBL2. The deepest penetrating residue is Asn^{189} from CBL1. Again, we identify approximate locations of atoms that may lead to favorable interactions such as H-bonding or electrostatic interaction. Residues Asn^{189} and Ser^{217} lie close to the phosphate plane. The η-nitrogen atoms in Arg^{216} and Arg^{249} might reach to the lipid phosphate although the α-carbon of these residues seems to be at the lipid-buffer interface. The polar Thr^{218} is located between the lipid phosphate and the lipid/buffer plane. The calcium ions Ca1 and Ca2 are located slightly closer to the negatively charged COO^- of the seryl group near the lipid-buffer interface than in the conformation shown in Fig. 6 *B*.

The structures in Fig. 6 and the description of the relative positions of the lipids and residues in the PKCα-C2 domain indicate that these two monolayer-bound structures interact differently with the lipid layer. These differences provide a qualitative basis to suggest that the PKCα-C2 domain in the $\theta = 35°$, $\varphi = 210°$ orientation is likely to have a more favorable interaction with the lipids because of the greater number of possibilities for hydrogen bonding and attractive electrostatic interactions. In support of this, the area of the docking surface for the $\theta = 35°$, $\varphi = 210°$ orientation (600 $Å^2$) is almost twice as large as that for the $\theta = 35°$, $\varphi = 0°$ orientation (340 $Å^2$), which also indicates a greater potential to interact with the lipids. On the basis of these

considerations, and biochemical mutational studies described below in the Discussion section, we have chosen the $\theta = 35°$, $\varphi = 210°$ orientation to describe the lipid-bound structure of the PKCα-C2 domain. In this orientation, the three CBLs dominate the membrane docking surface and among them CBL1 penetrates most deeply into the lipid monolayer.

DISCUSSION

Comparison to other results

In the proposed orientation ($\theta = 35°$, $\varphi = 210°$) the angle θ between the β2-strand vector and the membrane normal is 35°, which indicates that the monolayer-bound PKCα-C2 domain is oriented essentially perpendicular to the lipid layer as illustrated in Fig. 6 *A*. This orientation is inconsistent with the parallel orientation model proposed by crystallography and EPR measurements of PKCα-C2 domain binding to PC/PS membranes (Fig. 1 *B*) (6,25,26). X-ray crystallography studies of the PKCα-C2 domain bound to a short-chain PS, DCPS, suggested that only the central part of CBL3, *i.e.*, the side chains from residues Trp^{247} and Arg^{249}, is inserted into the lipid bilayer (6). This study also suggested that the β3-β4 connection of the PKCα-C2 domain, especially the residue Lys^{205}, approaches the membrane surface, but does not penetrate. Based on these crystallography results, Verdaguer et al. (6) proposed the parallel model in the docking of PKCα-C2/Ca^{2+}/DCPS complex. EPR studies (25,26) determined that the polar and charged Asn^{189}, Arg^{249}, and Arg^{252} side chains interact with polar and anionic groups inside the headgroup layer, but CBL2 does not penetrate the membrane. Results of the EPR study were used to suggest that the PKCα-C2 domain lies nearly parallel to the lipid layer with the longest β2-strand tilted at $68° \pm 7°$ from the membrane normal (26).

As discussed, our analysis of the x-ray reflectivity allows us to consider all orientations of the PKCα-C2 domain and, in particular, allows us to test if the orientations of the PKCα-C2 domain proposed by other authors would be compatible with our x-ray reflectivity data. In our notation, the orientation of the model proposed from x-ray crystallography is $\theta = 90°$, $\varphi = 300°$ and the orientation proposed from the EPR measurement (26) is $\theta = 68°$, $\varphi = 300°$. As shown in Fig. 4, these two orientations fit our x-ray reflectivity data unacceptably poorly, with their values greater than four standard deviations away from our best fits. In general, any approximately parallel orientation of the PKCα-C2 domain cannot provide an adequate fit to our data.

Although our proposed orientation for PKCα-C2 docking disagrees with that proposed from the x-ray crystallography and EPR studies, a number of important observations from the crystallography and EPR measurements agree with our proposed orientation. For example, the x-ray crystallography study observed that Asn^{189} and Arg^{216} residues interact with the lipid headgroup (6), which is consistent with our measurements. EPR measurements indicated that the polar and charged side chains of Asn^{189} and Arg^{249}, respectively, interact with polar and anionic groups inside the headgroup (25), also consistent with our measurements. Furthermore, our proposed docking model ($\theta = 35°$, $\varphi = 210°$, PEN = 7.5 Å) is supported by many mutational studies. In our model CBL1 penetrates deeply into the lipid headgroup, whereas CBL3 is positioned immediately adjacent to the lipid headgroups, but on the buffer side, as opposed to the parallel models for which the inverse is true. Our result is in agreement with a previous report showing that mutations of CBL1 ligands that coordinate to Ca1 had a more significant effect on vesicle binding than did mutations of CBL3 ligands that coordinate to Ca2 (15). Our result that CBL2 also penetrates the lipid headgroup, although to a lesser extent than CBL1, is consistent with the mutational study by Conesa-Zamora et al. (27) that observed that R216A of CBL2 affected both membrane binding and enzyme activation. CBL2 is not expected to interact with the membrane in the parallel models. The results of Conesa-Zamora et al. (27) that R249A and T251A of CBL3 affected both membrane binding and enzyme activation are also consistent with our results because these residues are located immediately adjacent to the lipid layer in our model. An important distinction between our model and the parallel models is the role of Lys^{205}. In our model, the Lys^{205} located in β3-β4 is far from the lipid monolayer and, therefore, is not important for the Ca^{2+}/PS-dependent binding. This arrangement is consistent with recent EPR (26) and mutagenesis (27) studies. For example, Conesa-Zamora et al. (27) concluded that Lys^{205} is essential neither for in vitro cellular membrane interaction of PKCα nor for PS-dependent enzyme activation.

It is sensible to expect that polar and charged residues that penetrate into the region of the lipid headgroup, and are therefore in direct contact with the headgroup, will have a stronger interaction with the membrane than those in the aqueous phase even if they are close to the lipid-water interface. In the $\theta = 35°$, $\varphi = 210°$ orientation, Asn^{189} in CBL1 penetrates into the lipid layer, indicating that it is likely to play some role in either the binding or the activation of the protein. In fact, Conesa-Zamora et al. (27) found that N189A mutant inhibited enzyme activity of PKCα. Bolsover et al. (17) showed that mutations of the side chains of Asn^{189} and Arg^{216} to Ala led to a weaker membrane association of the protein than did the same substitutions in Arg^{249} and Thr^{251}. An independent mutational study also showed that Asn^{189} plays a critical role in PS selectivity of PKCα (18). In addition, Arg^{216}, Arg^{249}, and Thr^{251} are also involved in PS binding (18,27). Later studies indicated that the mutation of Arg^{249} to Ala had no significant effect on the monolayer penetration (47). These results are all consistent with our bound structure shown in Fig. 6 *A*, which places Asn^{189} and Arg^{216} within the headgroup region and Arg^{249} and

Thr^{251} just outside. The importance of Arg^{216} provides further support for our choice of the bound structure shown in Fig. 6 *A* over that in Fig. 6 *B* because Arg^{216}, along with the rest of CBL2, does not penetrate the lipid layer in the configuration shown in Fig. 6 *B*.

Enzyme activation

PKCα contains three lipid binding domains, C1A and C1B, in addition to C2. A recent computational docking study of C1A and C2 interdomain interactions revealed a highly complementary interface that consists of Asp^{55}-Arg^{252} and Arg^{42}-Glu^{282} ion pairs and a Phe^{72}-Phe^{255} aromatic pair (47) (where the first residue of each pair is in C1A and the second is in C2). Mutation of Arg^{252}, Phe^{255}, and Glu^{282} to Ala suggested that these residues do not bind directly to the membrane, although they are involved in the interdomain interaction (47). As seen in Fig. 6 the backbone positions of Arg^{252}, Phe^{255}, and Glu^{282} (labeled in *blue*) do not penetrate into the lipid layer and are in a favorable position to interact with the C1A domain. As suggested by Stahelin et al. (47) this juxtaposing of the C1A domain with the membrane by the C2 domain should allow for further interaction of the C1A domain with the membrane and subsequent enzyme activation. Such arrangement is not achieved easily with parallel models.

A lysine-rich cluster, consisting of Lys^{197}, Lys^{199}, Lys^{209}, and Lys^{211} located in the area formed by the $\beta3$-$\beta4$-strands, has been recognized as a nonspecific binding site for phosphoinositides including PIP2 (22,48–50). Fig. 6 shows that this lysine-rich cluster is located on the periphery of the PKCα-C2 domain slightly more than halfway down its side. If the C2 domain would bind to PIP2 in the membrane, then it is expected that the angle θ would change from 35° (without PIP2) to ~50° (20,51) to yield a tilted orientation. The importance of this rotation is the possibility that it will push the C1A domain further into the lipid layer, allow C1A domain binding to DAG in the membrane, and lead to enzyme activation. In the $\theta = 35°$, $\varphi = 210°$ orientation, the C1A-C2 complementary pair that will interact first with the membrane as a result of the C2 rotation is likely to be Asp^{55}-Arg^{252} because it is located closest to the lipids. Interaction of the Asp^{55} and/or Arg^{252} with the membrane may lead to the untethering of the C1A domain and consequent enzyme activation. This is consistent with an earlier computational and mutational study (22,47). Direct evidence for such rotation could be provided by future x-ray reflectivity studies in which both PIP2 and PS are incorporated into the lipid layer.

SUMMARY

We have used x-ray reflectivity to determine the configuration of PKCα-C2 domains bound to a mixed monolayer of SOPC and SOPS lipids. A modification of our methodology introduced recently for analysis of x-ray reflectivity, that incorporates information from crystallographic studies, allowed us to consider efficiently all orientations of the protein domain in the analysis of the reflectivity data. This analysis led to two different bound structures illustrated in Fig. 6. Both are oriented nearly perpendicular to the lipid layer and penetrate partially into the lipid headgroup. Although these two configurations cannot be distinguished by x-ray reflectivity, qualitative consideration of the number and type of likely favorable interactions between the protein and the lipid headgroup led us to propose that the configuration in Fig. 6 *A* is the better representation of the two. The configuration shown in Fig. 6 *A* is consistent with many details of earlier EPR, crystallographic, and mutational studies, albeit in disagreement with the parallel bound orientation proposed from earlier studies. This configuration also exposes a lysine-rich cluster and other residues in a favorable location for further interactions with membrane PIP2 and the C1A domain, which would lead to tighter membrane binding and activation of PKCα.

SUPPORTING MATERIAL

X-ray data analysis methodology, complete PDB file, fluorescence microscopy, equations, two figures, a table, and references are available at http://www.biophysj.org/biophysj/supplemental/S0006-3495(09)01424-6.

C.H.C thanks Dr. Manoj Athavale and Binyang Hou for help with the analysis. M.L.S. thanks Dr. Aleksey Tikhonov for help with the X19C beamline at the National Synchrotron Light Source (Brookhaven National Laboratory). We thank Diana Murray for modifying the PDB file to include the additional residues from the purification protocol.

This work was supported by the National Science Foundation (CHE0315691 and CHE0615929 to M.L.S.), the National Institutes of Health (GM68849 and GM76581 to W.C.), ChemMatCARS, and the Department of Energy (Brookhaven National Laboratory and the National Synchrotron Light Source).

REFERENCES

1. DiNitto, J. P., T. C. Cronin, and D. G. Lambright. 2003. Membrane recognition and targeting by lipid-binding domains. *Sci. STKE*. 2003:re16.
2. Cho, W., and R. V. Stahelin. 2005. Membrane-protein interactions in cell signaling and membrane trafficking. *Annu. Rev. Biophys. Biomol. Struct.* 34:119–151.
3. Lomize, A. L., I. D. Pogozheva, M. A. Lomize, and H. I. Mosberg. 2007. The role of hydrophobic interactions in positioning of peripheral proteins in membranes. *BMC Struct. Biol.* 7:1–30.
4. Frazier, A. A., C. R. Roller, J. J. Havelka, A. Hinderliter, and D. S. Cafiso. 2003. Membrane-bound orientation and position of the synaptotagmin I C2A domain by site-directed spin labeling. *Biochemistry*. 42:96–105.
5. Ochoa, W. F., S. Corbalan-Garcia, R. Eritja, J. A. Rodriguez-Alfaro, J. C. Gomez-Fernandez, et al. 2002. Additional binding sites for anionic phospholipids and calcium ions in the crystal structures of complexes of the C2 domain of protein kinase Cα. *J. Mol. Biol.* 320:277–291.
6. Verdaguer, N., S. Corbalan-Garcia, W. F. Ochoa, I. Fita, and J. C. Gomez-Fernandez. 1999. Ca(2+) bridges the C2 membrane-binding domain of protein kinase Cα directly to phosphatidylserine. *EMBO J.* 18:6329–6338.

7. Xu, G. Y., T. McDonagh, H. A. Yu, E. A. Nalefski, J. D. Clark, et al. 1998. Solution structure and membrane interactions of the C2 domain of cytosolic phospholipase A2. *J. Mol. Biol.* 280:485–500.
8. Johnson, C. P., G. Fragneto, O. Konovalov, V. Dubosclard, J. F. Legrand, et al. 2005. Structural studies of the neural-cell-adhesion molecule by x-ray and neutron reflectivity. *Biochemistry.* 44:546–554.
9. Malkova, S., F. Long, R. V. Stahelin, S. V. Pingali, D. Murray, et al. 2005. X-ray reflectivity studies of cPLA2{alpha}-C2 domains adsorbed onto Langmuir monolayers of SOPC. *Biophys. J.* 89:1861–1873.
10. Malmberg, N. J., D. R. Van Buskirk, and J. J. Falke. 2003. Membrane-docking loops of the cPLA2 C2 domain: detailed structural analysis of the protein-membrane interface via site-directed spin-labeling. *Biochemistry.* 42:13227–13240.
11. Malkova, S., R. V. Stahelin, S. V. Pingali, W. Cho, and M. L. Schlossman. 2006. Orientation and penetration depth of monolayer-bound p40phox-PX. *Biochemistry.* 45:13566–13575.
12. Jiang, Y., M. Berk, L. S. Singh, H. Tan, L. Yin, et al. 2005. KiSS1 suppresses metastasis in human ovarian cancer via inhibition of protein kinase C alpha. *Clin. Exp. Metastasis.* 22:369–376.
13. Ng, T., D. Shima, A. Squire, P. I. Bastiaens, S. Gschmeissner, et al. 1999. PKCα regulates beta1 integrin-dependent cell motility through association and control of integrin traffic. *EMBO J.* 18:3909–3923.
14. Sun, X. G., and S. A. Rotenberg. 1999. Overexpression of protein kinase Cα in MCF-10A human breast cells engenders dramatic alterations in morphology, proliferation, and motility. *Cell Growth Differ.* 10:343–352.
15. Medkova, M., and W. Cho. 1998. Mutagenesis of the C2 domain of protein kinase C-alpha. Differential roles of Ca^{2+} ligands and membrane binding residues. *J. Biol. Chem.* 273:17544–17552.
16. Murray, D., and B. Honig. 2002. Electrostatic control of the membrane targeting of C2 domains. *Mol. Cell.* 9:145–154.
17. Bolsover, S. R., J. C. Gomez-Fernandez, and S. Corbalan-Garcia. 2003. Role of the Ca^{2+}/phosphatidylserine binding region of the C2 domain in the translocation of protein kinase Cα to the plasma membrane. *J. Biol. Chem.* 278:10282–10290.
18. Stahelin, R. V., J. D. Rafter, S. Das, and W. Cho. 2003. The molecular basis of differential subcellular localization of C2 domains of protein kinase C-alpha and group IVa cytosolic phospholipase A2. *J. Biol. Chem.* 278:12452–12460.
19. Evans, J. H., D. Murray, C. C. Leslie, and J. J. Falke. 2006. Specific translocation of protein kinase Cα to the plasma membrane requires both Ca^{2+} and PIP2 recognition by its C2 domain. *Mol. Biol. Cell.* 17:56–66.
20. Guerrero-Valero, M., C. Marin-Vicente, J. C. Gomez-Fernandez, and S. Corbalan-Garcia. 2007. The C2 domains of classical PKCs are specific PtdIns(4,5)P2-sensing domains with different affinities for membrane binding. *J. Mol. Biol.* 371:608–621.
21. Sanchez-Bautista, S., C. Marin-Vicente, J. C. Gomez-Fernandez, and S. Corbalan-Garcia. 2006. The C2 domain of PKCα is a Ca^{2+}-dependent PtdIns(4,5)P2 sensing domain: a new insight into an old pathway. *J. Mol. Biol.* 362:901–914.
22. Manna, D., N. Bhardwaj, M. S. Vora, R. V. Stahelin, H. Lu, et al. 2008. Differential roles of phosphatidylserine, PtdIns(4,5)P2, and PtdIns(3,4,5)P3 in plasma membrane targeting of C2 domains. Molecular dynamics simulation, membrane binding, and cell translocation studies of the PKCα C2 domain. *J. Biol. Chem.* 283:26047–26058.
23. Kohout, S. C., S. Corbalan-Garcia, A. Torrecillas, J. C. Gomez-Fernandez, and J. J. Falke. 2002. C2 domains of protein kinase C isoforms alpha, beta, and gamma: activation parameters and calcium stoichiometries of the membrane-bound state. *Biochemistry.* 41: 11411–11424.
24. Stahelin, R. V., and W. Cho. 2001. Roles of calcium ions in the membrane binding of C2 domains. *Biochem. J.* 359:679–685.
25. Kohout, S. C., S. Corbalan-Garcia, J. C. Gomez-Fernandez, and J. J. Falke. 2003. C2 domain of protein kinase C alpha: elucidation of the membrane docking surface by site-directed fluorescence and spin labeling. *Biochemistry.* 42:1254–1265.
26. Malmberg, N. J., and J. J. Falke. 2005. Use of EPR power saturation to analyze the membrane-docking geometries of peripheral proteins: applications to C2 domains. *Annu. Rev. Biophys. Biomol. Struct.* 34:71–90.
27. Conesa-Zamora, P., M. J. Lopez-Andreo, J. C. Gomez-Fernandez, and S. Corbalan-Garcia. 2001. Identification of the phosphatidylserine binding site in the C2 domain that is important for PKC alpha activation and in vivo cell localization. *Biochemistry.* 40:13898–13905.
28. Gidalevitz, D., Z. Huang, and S. A. Rice. 1999. Protein folding at the air-water interface studied with x-ray reflectivity. *Proc. Natl. Acad. Sci. USA.* 96:2608–2611.
29. Lee, K. Y., J. Majewski, T. L. Kuhl, P. B. Howes, K. Kjaer, et al. 2001. Synchrotron x-ray study of lung surfactant-specific protein SP-B in lipid monolayers. *Biophys. J.* 81:572–585.
30. Perisic, O., S. Fong, D. E. Lynch, M. Bycroft, and R. L. Williams. 1998. Crystal structure of a calcium-phospholipid binding domain from cytosolic phospholipase A2. *J. Biol. Chem.* 273:1596–1604.
31. Medkova, M., and W. Cho. 1998. Differential membrane-binding and activation mechanisms of protein kinase C-alpha and -epsilon. *Biochemistry.* 37:4892–4900.
32. Schlossman, M. L., D. Synal, Y. Guan, M. Meron, G. Shea-McCarthy, et al. 1997. A synchrotron x-ray liquid surface spectrometer. *Rev. Sci. Instrum.* 68:4372–4384.
33. Als-Nielsen, J., and D. McMorrow. 2001. Elements of Modern X-Ray Physics. John Wiley & Sons, New York.
34. Als-Nielsen, J., D. Jacquemain, K. Kjaer, F. Leveiller, M. Lahav, et al. 1994. Principles and applications of grazing incidence x-ray and neutron scattering from ordered molecular monolayers at the air-water interface. *Phys. Rep.* 246:251–313.
35. Pershan, P. S. 1990. Structure of surfaces and interfaces as studied using synchrotron radiation—liquid surfaces. *Faraday Discuss.* 89:231–245.
36. Gidalevitz, D., Y. Ishitsuka, A. S. Muresan, O. Konovalov, A. J. Waring, et al. 2003. Interaction of antimicrobial peptide protegrin with biomembranes. *Proc. Natl. Acad. Sci. USA.* 100:6302–6307.
37. Kent, M. S., H. Yim, J. K. Murton, D. Y. Sasaki, B. D. Polizzotti, et al. 2008. Synthetic polypeptide adsorption to Cu-IDA containing lipid films: a model for protein-membrane interactions. *Langmuir.* 24: 932–942.
38. Mohwald, H., H. Baltes, M. Schwendler, C. Helm, G. Brezesinski, et al. 1995. Phospholipid and protein monolayers. *Jpn. J. Appl. Phys.* 34:3906–3913.
39. Strzalka, J., X. Chen, C. C. Moser, P. L. Dutton, J. C. Bean, et al. 2001. X-ray scattering studies of Maquette peptide monolayers. 2. Interferometry at the vapor/solid interface. *Langmuir.* 17:1193–1199.
40. Zheng, S., J. Strzalka, C. Ma, S. J. Opella, B. M. Ocko, et al. 2001. Structural studies of the HIV-1 accessory protein Vpu in Langmuir monolayers: synchrotron X-ray reflectivity. *Biophys. J.* 80:1837–1850.
41. McGillivray, D. J., G. Valincius, F. Heinrich, J. W. Robertson, D. J. Vanderah, et al. 2009. Structure of functional *Staphylococcus aureus* alpha-hemolysin channels in tethered bilayer lipid membranes. *Biophys. J.* 96:1547–1553.
42. Lovell, S. C., I. W. Davis, W. B. Arendall, 3rd, P. I. de Bakker, J. M. Word, et al. 2003. Structure validation by Cα geometry: ϕ, ψ and Cβ deviation. *Proteins.* 50:437–450.
43. Bevington, P., and D. K. Robinson. 1992. Data Reduction and Error Analysis for the Physical Sciences. McGraw-Hill, New York.
44. Kucerka, N., J. F. Nagle, J. N. Sachs, S. E. Feller, J. Pencer, et al. 2008. Lipid bilayer structure determined by the simultaneous analysis of neutron and x-ray scattering data. *Biophys. J.* 95:2356–2367.
45. Wiener, M. C., and S. H. White. 1992. Structure of a fluid dioleoylphosphatidylcholine bilayer determined by joint refinement of x-ray and neutron diffraction data. III. Complete structure. *Biophys. J.* 61: 434–447.
46. Israelachvili, J. 1992. Intermolecular and Surface Forces. Academic Press, London.

47. Stahelin, R. V., J. Wang, N. R. Blatner, J. D. Rafter, D. Murray, et al. 2005. The origin of C1A–C2 interdomain interactions in protein kinase Cα. *J. Biol. Chem.* 280:36452–36463.

48. Corbalan-Garcia, S., J. Garcia-Garcia, J. A. Rodriguez-Alfaro, and J. C. Gomez-Fernandez. 2003. A new phosphatidylinositol 4,5-bisphosphate-binding site located in the C2 domain of protein kinase Cα. *J. Biol. Chem.* 278:4972–4980.

49. Marin-Vicente, C., F. E. Nicolas, J. C. Gomez-Fernandez, and S. Corbalan-Garcia. 2008. The PtdIns(4,5)P2 ligand itself influences the localization of PKCα in the plasma membrane of intact living cells. *J. Mol. Biol.* 377:1038–1052.

50. Rodriguez-Alfaro, J. A., J. C. Gomez-Fernandez, and S. Corbalan-Garcia. 2004. Role of the lysine-rich cluster of the C2 domain in the phosphatidylserine-dependent activation of PKCα. *J. Mol. Biol.* 335: 1117–1129.

51. Landgraf, K. E., N. J. Malmberg, and J. J. Falke. 2008. Effect of PIP2 binding on the membrane docking geometry of PKCα C2 domain: an EPR site-directed spin-labeling and relaxation study. *Biochemistry.* 47:8301–8316.

52. Heller, H., M. Schaefer, and K. Schulten. 1993. Molecular dynamics simulation of a bilayer of 200 lipids in the gel and in the liquid crystal phase. *J. Phys. Chem.* 97:8343–8360.